Modelling temperature effects on multiphase flow through porous media

Garth Wells, Tim Hooijkaas, Xuming Shan

Modelling temperature effects on multiphase flow through porous media

Journal:	*Philosophical Magazine & Philosophical Magazine Letters*
Manuscript ID:	TPHM-08-Apr-0107.R1
Journal Selection:	Philosophical Magazine
Date Submitted by the Author:	19-Sep-2008
Complete List of Authors:	Wells, Garth; University of Cambridge, Department of Engineering Hooijkaas, Tim; Shell International Exploration and Production Shan, Xuming; Delft University of Technology, Faculty of Civil Engineering and Geosciences
Keywords:	computer modelling, porous media
Keywords (user supplied):	computer modelling, porous media

Philosophical Magazine
Vol. 00, No. 00, 00 Month 200x, 1–14

RESEARCH ARTICLE

Modelling temperature effects on multiphase flow through porous media

Garth N. Wells[a]*, Tim Hooijkaas[b], Xuming Shan[c]

[a]Department of Engineering, University of Cambridge, United Kingdom
[b]Shell International Exploration and Production, Rijswijk, The Netherlands
[c]Faculty of Civil Engineering and Geosciences, Delft University of Technology, The Netherlands

(*Received 00 Month 200x; final version received 00 Month 200x*)

We consider strong temperature effects on two-phase immiscible flow through a porous medium. A dependency on temperature is introduced via a temperature-dependent viscosity for one of the phases. The purpose is to develop a simple prototype model for simulating the injection of steam into a porous medium which is saturated with highly viscous oil. To solve the problem, a Galerkin finite element model is formulated, with special residual-based terms added to stabilise the problem when advective transport processes dominate and to capture the discontinuities that develop at oil-water interfaces. It is also discussed how the mathematical representation of the numerical model can be transformed into computer code automatically, and two test cases are presented which demonstrate that this simplified model can capture typically observed phenomena robustly.

1. Introduction

The recovery of highly viscous hydrocarbons from reservoirs often relies on the introduction of significant quantities of heat into the system. The resulting increase in temperature dramatically reduces the viscosity of the hydrocarbon phase which then enhances flow through the porous medium due to the increased mobility of the oil phase. The modelling of this process is challenging on a number of fronts. The array of interacting physical processes is large and diverse, and the interactions between various processes must be properly captured. Furthermore, a number of the equations which model particular processes are difficult to solve numerically, demanding robust and flexible numerical solution strategies.

We consider here a simplified model for thermal recovery which retains phenomena that are both key in the real physical problem and are particularly challenging to solve robustly and stably with numerical methods. Our aim is to develop a robust, flexible and extensible variational framework which can capture the key physical processes during steam injection. The first step in this process is to develop a formulation which is capable of modelling essential processes, albeit in a highly simplified form, robustly. The simplified model we consider involves temperature dependent two-phase flow through a porous medium coupled to heat transport. While a number of effects are absent, numerically challenging aspects of the problem are retained.

Several example simulations are presented to demonstrate the model and to

*Corresponding author. Email: gnw20@cam.ac.uk

ISSN: 1478-6435 print/ISSN 1478-6443 online

DOI: 10.1080/1478643YYxxxxxxxx
http://www.informaworld.com

illustrate that effects which are crucial in the recovery of heavy oil can be captured. Large parts of the necessary computer code for the numerical examples have been generated using newly developed techniques for automated code generation. The numerical examples both support the proposed model as well as demonstrate the potential of automated computer modelling techniques for complex multi-physics problems.

The remainder of this work is organised as follows. The basic equations for two-phase flow through porous media and heat transport are presented in Section 2, which are followed in Section 3 by the proposed Galerkin finite element scheme. An overview of the automated modelling approach is given in Section 3.2, followed by numerical examples in Section 4, and conclusions are drawn in Section 5.

2. Governing equations for two-phase flow through a porous medium

We consider two-phase immiscible flow (oil/water) through a rigid porous medium. The domain of interest is denoted by $\Omega \subset R^d$, $1 < d \leq 3$, and it is fixed in space. The boundary of the domain Ω is denoted by $\partial\Omega$ and the outward unit normal vector on $\partial\Omega$ is denoted by $\boldsymbol{n}$. The overall medium has the porosity ϕ, and the fraction of the pore volume occupied by oil, the oil saturation, is denoted by S_o and the pore volume occupied by water, the water saturation, is denoted by S_w such that $S_o + S_w = 1$. It is assumed that no exchange of mass between the two phases can take place.

Some well-known equations for flow through porous media are briefly derived in order to shed some light on the assumptions which may require special consideration for fluids with high viscosity.

2.1. *Conservation of mass*

In the context of multiphase flow through a porous medium, mass conservation for the α-phase in the absence of a source term reads:

$$\frac{\partial \left(\phi \rho_\alpha S_\alpha\right)}{\partial t} + \nabla \cdot \left(\rho_\alpha \boldsymbol{u}_\alpha\right) = 0, \tag{1}$$

where ρ_α is the density of the α-phase, t denotes time and $\boldsymbol{u}_\alpha$ is the Darcy velocity of the phase α. The extension of Darcy's law to multiphase flow reads

$$\boldsymbol{u}_\alpha = -\frac{k_{r\alpha}\boldsymbol{\kappa}}{\mu_\alpha}\left(\nabla p_\alpha - \rho_\alpha \boldsymbol{g}\right), \tag{2}$$

where $k_{r\alpha}$ is the relative permeability of the α-phase, $\boldsymbol{\kappa}$ is the permeability tensor, p_α is the pressure in the α-phase and $\boldsymbol{g}$ is the acceleration due to gravity. Darcy flow can be derived from conservation of momentum under a number of assumptions and with an appropriate constitutive model [1]. A number of the necessary assumptions to arrive at Darcy's law from conservation of momentum are likely violated when considering heavy oil. In particular, the assumption underpinning Darcy flow that the fluid phases are macroscopically inviscid does not hold. Despite this, Darcy flow is still commonly adopted in practice for hydrocarbons with high viscosity.

We restrict our developments to two-phase flow, with $\alpha = o$ denoting the oil phase and with $\alpha = w$ denoting the water phase. Following the assumption of a rigid skeleton, $\partial\phi/\partial t = 0$, assuming that the oil and water phases are incompressible and assuming that the $p_o = p_w$ (zero capillary pressure, a common assumption for

heavy oil reservoirs), insertion of the Darcy velocity (2) into the mass conservation equation (1) leads to the elliptic continuity-like equation

$$\nabla \cdot [\lambda \boldsymbol{\kappa} \nabla p - (\lambda_o \rho_o + \lambda_w \rho_w) \boldsymbol{\kappa} \boldsymbol{g}] = 0, \tag{3}$$

where λ_α is the phase mobility,

$$\lambda_\alpha = \frac{k_{r\alpha}}{\mu_\alpha}, \tag{4}$$

and λ is the total mobility,

$$\lambda = \lambda_o + \lambda_w. \tag{5}$$

For the range of temperatures that we will be considering in the numerical examples, the validity of the incompressibility assumption is compromised. It does however lead to substantial simplifications while retaining key physical mechanisms, and in particular features which are challenging to model numerically.

The total velocity $\boldsymbol{u}$ is defined as

$$\boldsymbol{u} = \boldsymbol{u}_o + \boldsymbol{u}_w, \tag{6}$$

which is divergence-free under the assumptions of incompressible phases and $\partial\phi/\partial t = 0$. Using the expression for the phase velocities (2) in the conservation of mass equation (1) leads to an equation for the water saturation,

$$\phi \frac{\partial S}{\partial t} + \nabla \cdot (f \boldsymbol{u} + \boldsymbol{\kappa} \lambda_o f (\rho_w - \rho_o) \boldsymbol{g}) = 0, \tag{7}$$

where here and henceforth for notational convenience $S = S_w$, and f is the fractional flow function for the water phase,

$$f = \frac{\lambda_w}{\lambda}. \tag{8}$$

Using incompressibility of the total velocity $\boldsymbol{u}$ leads to the well-known Buckley-Leverett equation,

$$\phi \frac{\partial S}{\partial t} + f_{,S} \boldsymbol{u} \cdot \nabla S + \nabla \cdot (\boldsymbol{\kappa} \lambda_o f (\rho_w - \rho_o) \boldsymbol{g}) = 0, \tag{9}$$

where $f_{,S} = \partial f / \partial S$. The saturation equation is nonlinear since f will depend on S, and due to the assumption of zero capillary pressure it is purely hyperbolic. The saturation equation admits shocks, which represent an oil–water interface. The numerical treatment of the advective term is often a delicate point when working with advective fields which are solenoidal in the exact case since in computations it is possible that the advective velocity field is not locally divergence-free. A discussion of this issue in the context of Galerkin and stabilised finite elements methods can be found in Ref. [2].

2.2. *Conservation of energy*

In considering conservation of energy, kinetic and potential energy are neglected, and the liquid phases are assumed to be macroscopically inviscid. Furthermore,

under the assumption that no momentum transfer takes place between phases, conservation of energy reads

$$\frac{\partial}{\partial t}\left[\phi\sum_{\alpha}\rho_{\alpha}H_{\alpha}S_{\alpha}+(1-\phi)\,\rho_{s}H_{s}\right]+\nabla\cdot\left(\sum_{\alpha}\rho_{\alpha}H_{\alpha}\boldsymbol{u}_{\alpha}\right)-\nabla\cdot k_{T}\nabla T=0, \quad (10)$$

where the solid phase is denoted by the subscript s, $\alpha = o, w$, H_α is the enthalpy per unit mass of phase α, ρ_s is the mass density of the solid skeleton and H_s is the enthalpy of the solid skeleton. The scalar k_T is an 'equivalent' thermal conductivity. Following [3] and consistent with incompressibility of the phases, we ignore the work done by the pressure and set $H_\alpha = U_\alpha$, where U_α is the internal energy of the α-phase. Using conservation of mass (1), the conservation of energy expression can be rephrased as

$$\phi\sum_{\alpha}\rho_{\alpha}S_{\alpha}\frac{\partial H_{\alpha}}{\partial t}+(1-\phi)\,\frac{\partial\left(H_{s}\rho_{s}\right)}{\partial t}+\sum_{\alpha}\nabla H_{\alpha}\cdot\left(\rho_{\alpha}\boldsymbol{u}_{\alpha}\right)-\nabla\cdot\left(k_{T_{t}}\nabla T\right)=0. \quad (11)$$

The specific heat C_α is defined as dH_α/dT, which leads to

$$M\frac{\partial T}{\partial t}+\left(\rho_{o}C_{o}\boldsymbol{u}_{o}+\rho_{w}C_{w}\boldsymbol{u}_{w}\right)\cdot\nabla T-\nabla\cdot\left(k_{T_{t}}\nabla T\right)=0, \quad (12)$$

where

$$M=\phi\sum_{\alpha}\rho_{\alpha}C_{\alpha}S_{\alpha}+(1-\phi)\,\rho_{s}C_{s}. \quad (13)$$

Under the assumptions $\rho C = \rho_o C_o = \rho_w C_w = \rho_s C_s$, the conservation of energy expression reduces to the conventional advective-diffusive scalar transport equation,

$$\frac{\partial T}{\partial t}+\boldsymbol{u}\cdot\nabla T=\nabla\cdot\nu\nabla T, \quad (14)$$

where $\nu = k_{T_t}/\rho C$. We consider this highly simplified form of conservation of energy as it still possesses a number of key features and is difficult to solve numerically when advective transport dominates.

2.3. *Temperature dependencies*

Various terms in the model can be made temperature dependent. When modelling thermal recovery methods, we will consider a strong dependency of the oil viscosity on the temperature. The precise nature of this dependency is presented with the relevant examples.

3. Galerkin finite element formulation

We develop a finite element formulation with a view to more complex models which will incorporate more physical phenomena and more fields. This mandates the use of staggered solution procedures as it will most certainly not be tractable to solve all fields in a coupled fashion. Where necessary stabilisation techniques are employed and the computer code is generated largely automatically using a variational form compiler.

3.1. *Galerkin problems*

The domain of interest is triangulated into n non-overlapping elements E_i such that $\bar{\Omega} = \bigcup_{i=1}^{n} \bar{E}_i$. The boundary $\Gamma = \partial\Omega$ is partitioned such that: $\Gamma = \overline{\Gamma_p \bigcup \Gamma_u}$, $\Gamma_p \bigcap \Gamma_u = \emptyset$; $\Gamma_S \subset \Gamma$; and $\Gamma = \overline{\Gamma_T \bigcup \Gamma_q}$, $\Gamma_T \bigcap \Gamma_q = \emptyset$; Before proceeding with the various formulations, it is useful to define some function spaces. Consider

$$P = \left\{p \in H^1(\Omega) : p \in P^2(E_i) \ \forall\, i,\ p = 0 \text{ on } \Gamma_p\right\}, \tag{15}$$

$$P^\star = \left\{p \in H^1(\Omega) : p \in P^2(E_i) \ \forall\, i,\ p = g_p \text{ on } \Gamma_p\right\}, \tag{16}$$

$$U = \left\{u \in H^1(\Omega) : u \in P^1(E_i) \ \forall\, i,\ u = 0 \text{ on } \Gamma_S\right\}, \tag{17}$$

$$U^\star = \left\{u \in H^1(\Omega) : u \in P^1(E_i) \ \forall\, i,\ u = g_S \text{ on } \Gamma_S\right\}, \tag{18}$$

$$V = \left\{v \in H^1(\Omega) : v \in P^1(E_i) \ \forall\, i,\ v = 0 \text{ on } \Gamma_T\right\}, \tag{19}$$

$$V^\star = \left\{v \in H^1(\Omega) : v \in P^1(E_i) \ \forall\, i,\ v = g_T \text{ on } \Gamma_T\right\}, \tag{20}$$

where L^2 is the space of square-integrable functions, H^1 is the Sobolev space of functions with square-integrable derivatives, $P^k(E_i)$ defines Lagrange finite element basis functions of order k on the element E_i, and g_p, g_S and g_T are prescribed. In the context of the differential equations that we are considering, the last three terms will be associated with Dirichlet boundary conditions.

In reservoir simulation, $H(\mathrm{div}, \Omega)$ elements [4] are often used to guarantee local mass conservation and to improve the accuracy of the velocity field. We have chosen to work with conforming Lagrange basis functions and not to solve the Darcy flow problem in a mixed fashion. In attempting to maintain the quality of the velocity field, we will use quadratic basis functions for the pressure field. Determination of the most appropriate strategy, particularly when compressible phases are considered, is a topic which requires further investigation.

The Galerkin problem corresponding to the pressure equation (3) reads: given λ^n, λ_o^n, λ_w^n, h_u^{n+1}, find $p^{n+1} \in P^\star$ such that

$$-\int_\Omega \nabla q \cdot \lambda^n \boldsymbol{\kappa} \nabla p^{n+1}\, d\Omega = -\int_\Omega \nabla q \cdot \left(\left(\lambda_o^n \rho_o + \lambda_w^n \rho_w\right) \boldsymbol{\kappa} \boldsymbol{g}\right)\, d\Omega + \int_{\Gamma_u} q h_u^{n+1}\, d\Gamma_u \quad \forall\, q \in P, \tag{21}$$

where Γ_u is the part of the boundary upon which the normal component of the total velocity is specified, and h_u^{n+1} is the prescribed normal velocity at time t^{n+1}. Using p^{n+1}, the phase velocities and total velocity are updated according to Darcy's law (2), yielding $\boldsymbol{u}_o^{n+1}$, $\boldsymbol{u}_w^{n+1}$ and $\boldsymbol{u}^{n+1}$. The saturation equation (9) and the heat transport (14) equation are then solved using the updated advective velocity $\boldsymbol{u}^{n+1}$.

A stabilised Galerkin problem for the saturation equation using the streamline upwind Petrov-Galerkin method [5] and shock-capturing operator reads: given S^n,

$f^n_{,S}$, f^n, $\boldsymbol{u}^{n+1}$ and λ^n_o, find $S^{n+1} \in U^\star$ such that

$$\int_\Omega v\phi\frac{S^{n+1}-S^n}{\Delta t}\,d\Omega + \int_\Omega v f^n_{,S}\boldsymbol{u}^{n+1}\cdot\nabla S^{n+1}\,d\Omega + \sum_{E_i}\int_{E_i}\left(\boldsymbol{u}^{n+1}\cdot\nabla v\right)\tau_s r^{n+1}\,d\Omega + \sum_{E_i}\int_{E_i}\nu_{\text{shock}}\nabla v\cdot\nabla S^{n+1}\,d\Omega = -\int_\Omega v\nabla\cdot\left(\boldsymbol{\kappa}\lambda^n_o f^n\left(\rho_w-\rho_o\right)\boldsymbol{g}\right)\,d\Omega \quad \forall\, v\in U, \quad (22)$$

where $\sum_{E_i}\int_{E_i}(\cdot)$ indicates integration over all element interiors, r^{n+1} is the residual at time step $n+1$,

$$r^{n+1} = \phi\frac{S^{n+1}-S^n}{\Delta t} + f^n_{,S}\boldsymbol{u}^{n+1}\nabla S^{n+1} + \nabla\cdot\left(\boldsymbol{\kappa}\lambda^n_o f^n\left(\rho_w-\rho_o\right)\boldsymbol{g}\right). \quad (23)$$

and τ_s is a stabilisation parameter which is defined element-wise. We have adopted

$$\tau_s = \frac{h}{2\|\boldsymbol{u}^{n+1}\|} \quad (24)$$

where h is a measure of the element size. This expression is well-accepted for purely hyperbolic problems [6]. The term ν_{shock} is an artificial shock viscosity defined as

$$\nu_{\text{shock}} = \begin{cases} \dfrac{\beta h|r^{n+1}|}{2\|\nabla S^n\|} & \text{if } \|\nabla S^n\|\neq 0, \\ 0 & \text{otherwise,}\end{cases} \quad (25)$$

where β is a parameter. This artificial shock viscosity was proposed by Codina [7], although we have not adopted an anisotropic version. Based on numerous numerical experiments, some of which are reported in Section 4, a value of $\beta = 2$ has been found to be effective in that jumps in the solution are typically spread across two elements. Oscillations about discontinuities are avoided without overly smoothing the front. We note that both stabilisation terms in the variational problem are residual based, i.e. they vanish for the exact solution. For purely hyperbolic problems, a variety of specialised and effective numerical methods exist. We have deliberately chosen a generic approach as it can be extended to more general cases in which the saturation equation is not purely hyperbolic.

Finally, for the heat transport problem, the stabilised Galerkin problem reads: given T^n and $\boldsymbol{u}^{n+1}$, find $T^{n+1}\in V^\star$ such that

$$\int_\Omega w\frac{T^{n+1}-T^n}{\Delta t}\,d\Omega + \int_\Omega w\boldsymbol{u}^{n+1}\cdot\nabla T^{n+1}\,d\Omega + \int_\Omega\nabla w\cdot\nu\nabla T^{n+1}\,d\Omega + \sum_E\int_E\boldsymbol{u}^{n+1}\cdot\nabla w\tau_{\text{T}}r^{n+1}_{\text{T}}\,d\Omega = \int_{\Gamma_q} w h^{n+1}_q\,d\Gamma \quad \forall\, w\in V, \quad (26)$$

where Γ_q is the part of the boundary on which the diffusive heat flux is prescribed and h^{n+1}_q is the prescribed diffusive heat flux at time t^{n+1}. For the heat equation, we adopt a definition of the stabilisation parameter which takes into account the

presence of a diffusive term [8],

$$\tau_{\mathrm{T}} = \left(1 - \frac{1}{Pe}\right)^{-1} \frac{h}{2\|\boldsymbol{u}^{n+1}\|}, \tag{27}$$

where element Péclet number $Pe = \left\|\boldsymbol{u}^{n+1}\right\| h/2\nu$. The residual associated with the heat transport equation reads

$$r_T^{n+1} = \frac{T^{n+1} - T^n}{\Delta t} + \boldsymbol{u}^{n+1} \cdot \nabla T^{n+1} - \nabla \cdot \nu \nabla T^{n+1}. \tag{28}$$

With the new water saturation and temperature, all quantities which are dependent on the saturation and the temperature are updated, and the procedure is advanced in time and repeated.

In summary, the solution procedure involves:

Algorithm 1:

(1) Solve the pressure equation (21).
(2) Compute the Darcy velocity.
(3) Solve the saturation (22) and heat transport (26) equations.
(4) Update the fractional flow functions, viscosities and densities, and advance in time.

Each field is decoupled in the solution process, and at each step an implicit solution procedure is adopted. The problem is linearised about the previous time step and advanced in time. It is likely that such a procedure will only be first-order accurate in time regardless of the time stepping scheme used for each equation, therefore we have used the backward Euler approach. Experience from the simulation of various problems indicates that the stabilised scheme is particularly robust. To gain further insights into the stability, conservation and accuracy properties of the procedure, detailed *a priori* analysis is required.

A significant number of numerical solution procedures are used in reservoir engineering, and an overview of some common approaches can be found in Ref. [9]. Noteworthy is that variational methods are relatively novel in this context.

3.2. *Automated computer code generation*

Numerical models and the resulting computer code for modelling enhanced recovery methods for heavy oil are marked by complexity and diversity. This makes the problem a candidate for exploring the potential of automated computer code generation for solving differential equations. We have therefore developed computer code for the proposed model using recent developments from the FEniCS Project [10]. In particular, the FEniCS Form Compiler (FFC) [11, 12] is used to generate the computer code required for computing the generating element matrices and vectors, and the library DOLFIN [13] is used to assemble and solve the resulting equations. All components of the FEniCS Project are licenced under a GNU Public License or a Lesser GNU Public License and can be found at `www.fenics.org`.

The form compiler FFC produces low-level code from a high-level input which resembles mathematical notation. By default, FFC will produce C++ output consistent with the Unified Form-assembly Code format (UFC) [14]. The automatically generated code can be used in combination with any library that supports the UFC format, such as DOLFIN. The compiler approach for variational forms permits various *a priori* optimisations. A number of optimisations are are employed,

such as alternative element tensor representations [11] and loop unrolling. Particularly appealing is that mixed function spaces can be used trivially in the context of multi-physics problems. Using an automated modelling approach which mirrors mathematical formulations, models can be easily and rapidly extended and modified, and the resulting code is potentially faster than hand-optimised specialised code.

4. Numerical examples

Two example problems are presented to illustrate the model and the physical processes that we wish to simulate. Both use unstructured meshes with triangular elements. This permits the consideration of complex geometries and opens the possibility of using spatially adaptive schemes which are attractive in the context of thermal recovery modelling.

4.1. *Model parameters*

For all examples, the Corey model [15] for the relative permeability is used. For this model the relative permeabilities read

$$k_{rw} = k_{rw,end}\left(\frac{S - S_{wc}}{1 - S_{wc} - S_{or}}\right)^{n_w}, \tag{29}$$

$$k_{ro} = \left(\frac{1 - S - S_{or}}{1 - S_{wc} - S_{or}}\right)^{n_o}, \tag{30}$$

where $k_{rw,end}$ is the water relative permeability when $S = 1 - S_{or}$, where S_{or} is the irreducible oil saturation, S_{wc} is the connate water saturation and the exponents n_w and n_o are model parameters. For all examples we adopt $S_{wc} = 0.15$, $S_{or} = 0.15$, $n_w = 3.5$, $n_o = 1.5$ and $k_{rw,end} = 0.5$.

The viscosity of typical heavy oil drops exponentially with increasing temperature. We therefore adopt the relationship

$$\mu_o = c_1\left(T/T^{\text{ref}}\right)^{-c_2}, \tag{31}$$

where $c_1 > 0$, $c_2 \geq 0$ and $T^{\text{ref}} > 0$.

4.2. *Water flooding*

The case of water flooding in a rectangular domain is simulated to examine the performance of the model in the presence of shocks in the saturation field. A rectangular domain $\Omega = (0, 3) \times (0, 1)$ (length units of metres) is considered, with the pressure set equal to 100 Nm^{-2} at the inflow boundary and zero at the outflow boundary,

$$p = \begin{cases} 100 & \text{if } x_1 = 0, \\ 0 & \text{if } x_1 = 3, \end{cases} \tag{32}$$

and no net flow is permitted in the x_2 direction,

$$\boldsymbol{u} \cdot \boldsymbol{n} = 0 \quad \text{if } x_2 = 0 \text{ or } x_2 = 1. \tag{33}$$

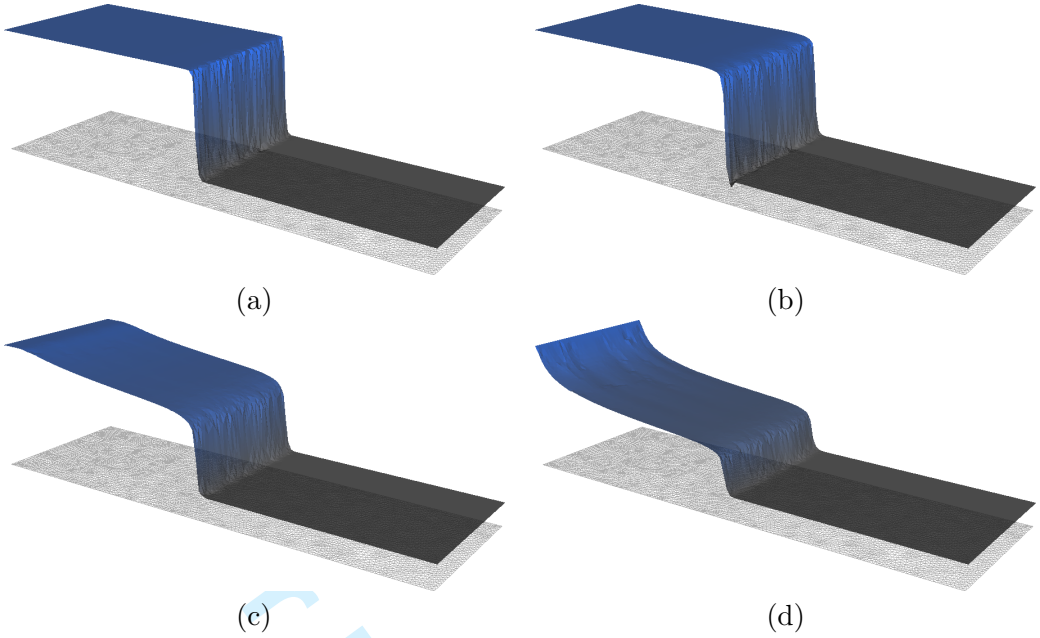

Figure 1. Water saturation profiles for the water flooding test case for (a) $\mu_o/\mu_w = 0.1$; (b) $\mu_o/\mu_w = 1$; (c) $\mu_o/\mu_w = 10$; and (d) $\mu_o/\mu_w = 100$.

For the saturation equation, the initial saturation $S(\boldsymbol{x}, 0) = 0.15$ and the saturation on the boundary at $x_1 = 0$ is increased from 0.15 to 0.8 linearly as a function of time over 10 time increments. Gravity effects are neglected, porosity $\phi = 1$, permeability $\boldsymbol{\kappa} = \boldsymbol{I}$ m^2 and temperature effects are not included. For the water phase $\mu_w = 1$ Nsm^{-2}, and the oil viscosity is varied for four tests. For $\mu_o/\mu_w = 0.1$, $\Delta t = 5 \times 10^{-4}$ s; $\mu_o/\mu_w = 1$, $\Delta t = 1 \times 10^{-3}$ s; $\mu_o/\mu_w = 10$, $\Delta t = 2.5 \times 10^{-3}$ s; and $\mu_o/\mu_w = 100$, $\Delta t = 1 \times 10^{-2}$ s. The time steps are chosen such that the water-oil interfaces travel half the domain in a comparable number of time steps.

Figure 1 shows the saturation profiles for the various oil–water viscosity ratios at the time at which the water-oil interface is located approximately at the mid-point of the domain. The elevation indicates the water saturation, and in all cases it is equal to 0.8 at the left-hand boundary and 0.15 at the right-hand boundary. For all viscosity ratios, the shock is spread over approximately two cells and no overshoot can be observed behind the water–oil interface. Minimal overshoot can be observed in front of the shock in some cases. This could be attributed to the 'time lag' in the computation of the shock capturing viscosity.

4.3. *Steam assisted gravity drainage prototype*

The example in this section aims to qualitatively reproduce the basic processes active during a more complex process which is known as steam assisted gravity drainage (SAGD) [16]. SAGD involves the injection of steam at a horizontal injection well, with a horizontal production well placed below the injection well. Driven by buoyancy effects, heat is transported upwards, resulting in a dramatic drop in oil viscosity. Then, due to the increased mobility of the oil and the influence of gravity, oil flows downwards towards the production well.

The reservoir configuration to be modelled is shown in Figure 2. Two wells are visible at the centre of Figure 2. The upper well is the injection well and the lower well is the production well. The lower well is located 4 m from the bottom of the domain, and the distance between the injection and production wells is 6 m. Hot

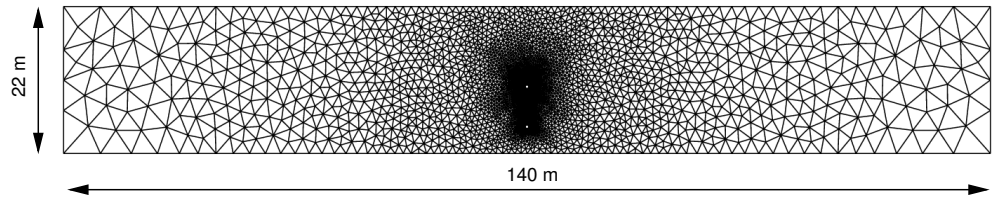

Figure 2. Problem geometry for the SAGD-like test case.

water is injected at the injection well. Two cases are considered: the first involving a negligible imposed pressure gradient between the wells and strong buoyancy effects; and the second involving an induced pressure gradient between the wells and no buoyancy effects. In both cases, the initial water saturation is set to $S(\boldsymbol{x}, 0) = 0.32$ and the initial temperature $T(\boldsymbol{x}, 0) = 15$ °C. The oil density $\rho_0 = 1.1 \times 10^3$ kgm^{-3} and the water density $\rho_w = 1.0 \times 10^3$ kgm^{-3}. Both are held constant. The oil viscosity evolves according to equation (31) with $c_1 = 2.77 \times 10^6$Nsm^2, $c_2 = -3.74$, and $T^{\text{ref}} = 1$ °C. The water viscosity is kept constant at $\mu_w = 8.4 \times 10^{-4}$ Nsm^{-2}, and the thermal diffusivity is constant at $\nu = 6.16 \times 10^{-7}$ m^{2}s^{-1}.

Pertinent to the pressure equation, the pressure is prescribed at the injection and production wells, and no flow is permitted ($\boldsymbol{u} \cdot \boldsymbol{n} = 0$) at the top, bottom and sides of the domain. For the saturation equation, the water saturation S is prescribed at the injection well where it is increased linearly as a function of time from 0.15 to 0.84 over 80 time increments and is then held constant. All other boundaries are outflow or no-flow, hence the saturation is not prescribed. For the heat equation, the temperature is prescribed at the injection well, and is increased linearly as a function of time from 15 °C up to 200 °C over 80 time steps and is then held constant. At all other boundaries, the diffusive heat flux across the boundary is set to zero and the advective flux is not prescribed as they are no-flow or outflow boundaries. A constant time step of $\Delta t = 1.25 \times 10^3$ s is used.

For the first example, buoyancy effects are exaggerated by setting $g = 9.81 \times 10^3$ ms^{-2}. The pressure $p = 4.4 \times 10^6$ Nm^{-2} at the injection well and $p = 4.39 \times 10^6$ Nm^{-2} at the recovery well. Therefore the externally imposed pressure gradient between the wells is negligible.

The evolution of the water saturation for this problem is shown in Figure 3. The oil in a significant region around the injection well has been displaced by water and recovered. The processes involved can be further elucidated by considering the evolution of the temperature field, shown in Figure 4. The warm region mirrors closely the displaced oil region. Heat has been transported upwards by the water phase which moves upwards due to buoyancy. The rise in temperature causes a drop in the oil viscosity and oil then flows downwards, as shown in Figure 5 at various time steps. In Figure 5, the contours indicate the magnitude of the oil velocity and the arrows indicate the direction. Clearly, the oil velocity is highest at the boundaries of the heated zone. Gravity drives the oil towards the production well. As the recovery process proceeds, the effectiveness of the gravity driving force is reduced as the flow direction transitions from near vertical towards the horizontal.

This problem has also been computed with a mesh that has been refined by a factor of two in both directions. The computed results resemble each other closely, and as one would reasonably expect with a refined mesh, the oil-water interface is sharper.

The second example examines the response in the presence of an imposed pressure gradient between the two wells and the absence of buoyancy effects. For this problem, $p = 4.4 \times 10^6$ Nm^{-2} at the injection well and $p = 0$ at the production well, and $\rho_o = \rho_w$. The water saturation and the temperature field are shown in Figure 6

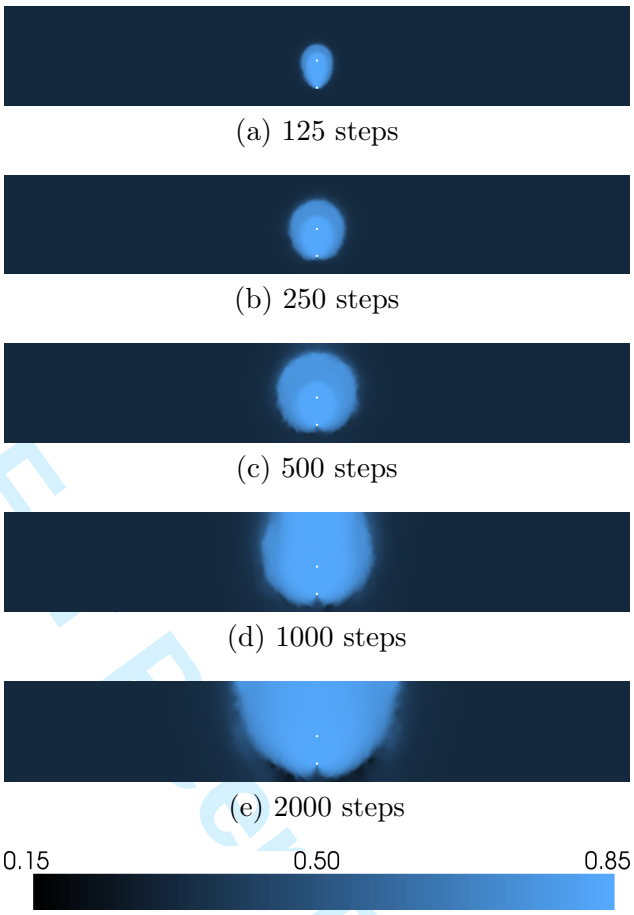

Figure 3. Evolution of the water saturation S in the presence of negligible imposed pressure gradient.

after 2000 time steps. Clearly, oil has been recovered primarily from the region between the two wells and the recovered domain is far smaller compared with the gravity assisted case (see Figure 3). The small recovery domain is reflected in the temperature field. Most of the injected heat is transported directly towards the production well. This can be seen by examining the water velocity field shown in Figure 7. Similar to the oil velocity plots, in Figure 7 the contours indicate the magnitude of the water velocity and the arrows indicate the direction of the flow. Much of the heated water which is injected moves directly to the production well and the region from which oil is recovered does not evolve. This phenomena can be reinforced if the geomechanical response is considered, as the high flow velocity between the wells can lead to a reduction in porosity. This is particularly the case for heavy oils as they are usually found in cohesion-less sands rather than the more typical porous rocks.

5. Conclusions

A stabilised Galerkin formulation has been presented for modelling temperature effects on two-phase flow through porous media. It represents a simplified model for thermal oil recovery techniques and provides a platform for further developments in modelling steam injection into porous media. The Galerkin finite element approach has been chosen as it naturally permits the use of unstructured grids and extends naturally to various different equations which will play a role in more sophisticated models incorporating more interacting processes.

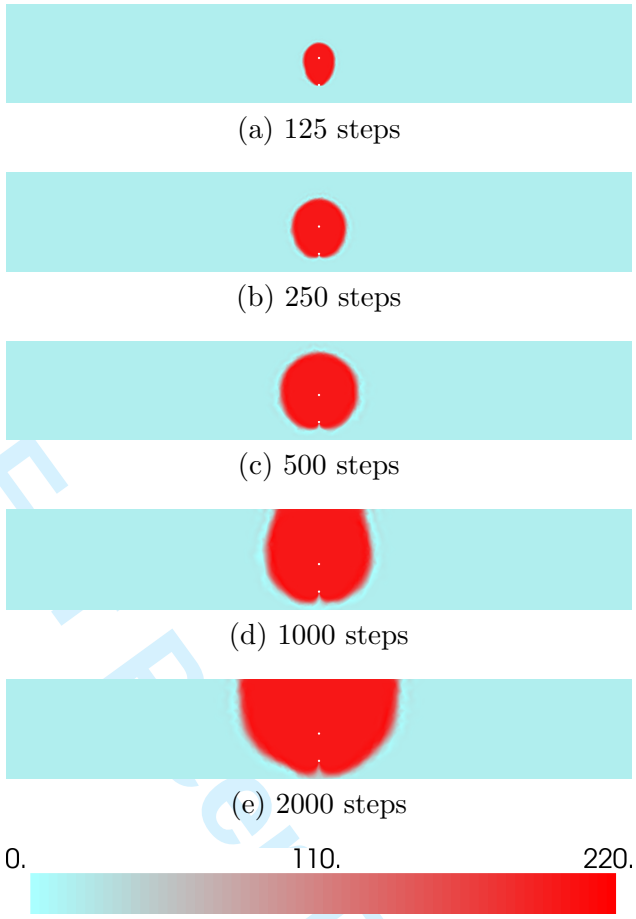

Figure 4. Evolution of the temperature field T in the presence of negligible imposed pressure gradient.

Stabilisation techniques have been used to deal with the difficulties which arise when advection dominated transport processes are involved and a shock capturing term has been used to deal with the discontinuity at the oil–water interface which arises due to the assumption of zero capillary pressure. These residual-based stabilisation techniques have led to stable results, but such methods must be used with care as it is possible that important physical instabilities are being suppressed. In particular, one may expect fingering when displacing a phase with another phase which is significantly more mobile, and stabilisation schemes may suppress this phenomenon. This point is deserving of further attention.

Finally, the complexity of the thermal recovery process and the resulting computer models places a heavy burden on software development. Therefore we have investigated the application of new automated code generation techniques and shown by example that automation concepts and tools can be applied for such problems. These tools are in fact extremely useful for these types of models to speed the development process, produce potentially faster computer code, and they provide a high degree of flexibility to rapidly experiment with different models and numerical formulations.

Acknowledgements

Part of this research was carried out within the context of the ISAPP Knowledge Centre. ISAPP (Integrated Systems Approach to Petroleum Production) is a joint project of the Netherlands Organisation for Applied Scientific Research TNO, Shell

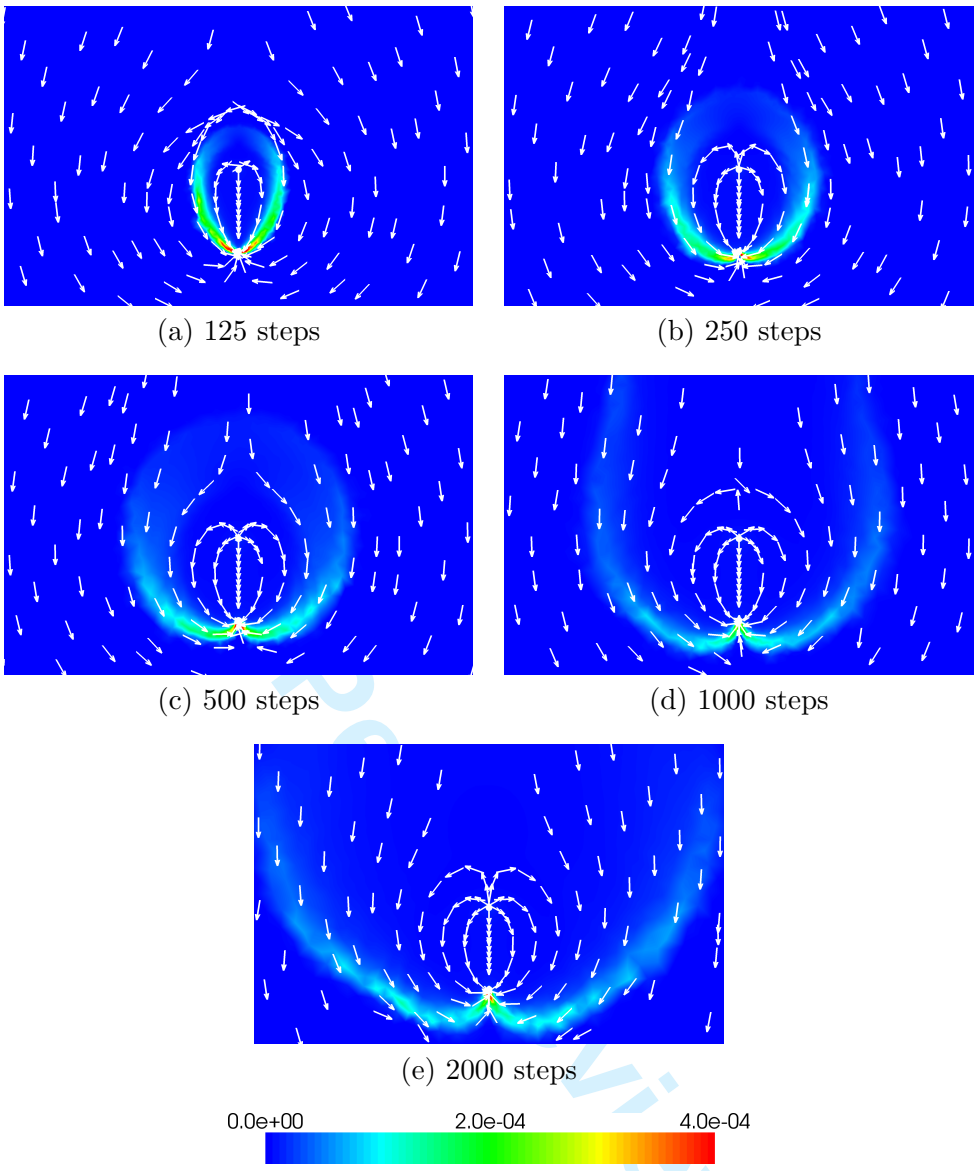

Figure 5. Evolution of oil velocity field $\boldsymbol{u}_o$ in the presence of negligible imposed pressure gradient.

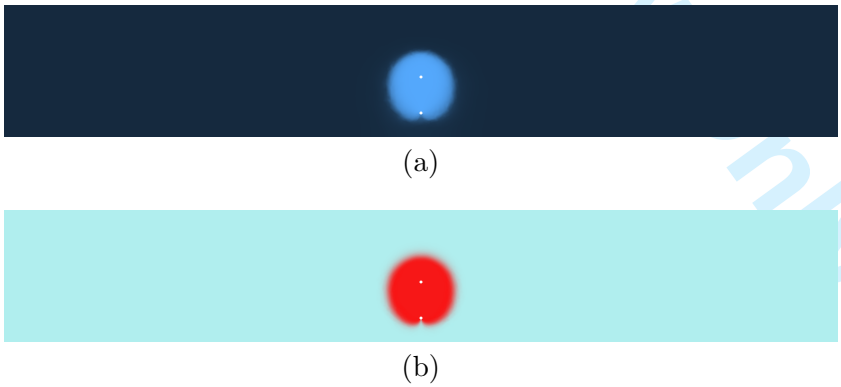

Figure 6. Contours of the (a) water saturation S and (b) temperature field T in the presence of a significant induced pressure gradient after 2000 steps.

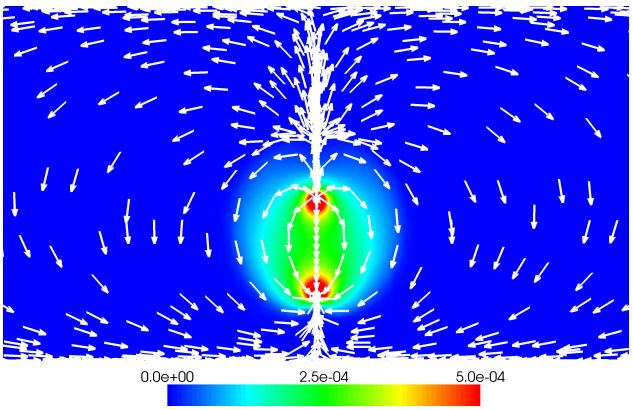

Figure 7. Water velocity $\boldsymbol{u}_w$ in the presence of a significant pressure differential after 2000 time steps.

International Exploration and Production, and Delft University of Technology.

References

[1] M. Hassanizadeh and W.G. Gray, *General conservation equations for multi-phase systems: 3. Constituive theory for porous media flow*, Advances in Water Resources 3 (1980), pp. 25–40.
[2] T.J.R. Hughes and G.N. Wells, *Conservation properties for the Galerkin and stabilised forms of the advection-diffusion and incompressible Navier-Stokes equations*, Computer Methods in Applied Mechanics and Engineering 194(9–11) (2005), pp. 1141–1159.
[3] L.W. Lake *Enhanced Oil Recovery*, Prentice-Hall, New Jersey, 1989.
[4] F. Brezzi and M. Fortin *Mixed and Hybrid Finite Element Methods*, Springer-Verlag, New York, 1991.
[5] A.N. Brooks and T.J.R. Hughes, *Streamline upwind Petrov-Galerkin formulations for convection dominated flows with particular emphasis on the incompressible Navier-Stokes equations*, Computer Methods in Applied Mechanics and Engineering 32(1–3) (1982), pp. 199–259.
[6] J. Donea and A. Huerta *Finite Elements Methods for Flow Problems*, John Wiley and Sons Ltd, Chichester, United Kingdom, 2003.
[7] R. Codina, *A discontinuity-capturing crosswind-dissipation for the finite element solution of the convection-diffusion equation*, Computer Methods in Applied Mechanics and Engineering 110(3–4) (1993), pp. 325–342.
[8] R. Codina, *On stabilized finite element methods for linear systems of convection-diffusion-reaction equations*, Computer Methods in Applied Mechanics and Engineering 188(1–3) (2000), pp. 61–82.
[9] Z. Chen, G. Huan, and Y. Ma *Computational Methods for Multiphase Flows in Porous Media*, Society for Industrial and Applied Mathemcatics (SIAM), Philadelphia, 2006.
[10] The FEniCS Project; `www.fenics.org`.
[11] R.C. Kirby and A. Logg, *A Compiler for Variational Forms*, ACM Transactions on Mathematical Software 32(3) (2006), pp. 417–444.
[12] K.B. Ølgaard, A. Logg, and G.N. Wells, *Automated code generation for discontinuous Galerkin methods*, SIAM Journal on Scientific Computing (2008) To appear.
[13] A. Logg et al. *DOLFIN User Manual*, , 2008 URL: `http://www.fenics.org/dolfin/`.
[14] M. Alnæs et al., UFC Specification and User Manual; URL: `http://www.fenics.org/ufc/`.
[15] A.T. Corey *Mechanics of Immiscible Fluids in Porous Media*, Water Resource Publications, Colorado, 1986.
[16] R.M. Butler *Thermal Recovery of Oil and Bitumen*, Prentice-Hall, 1991.